Experimental Evidence of a Nonlinear Transition from Convective to Absolute Instability

P. Gondret, P. Ern, L. Meignin, and M. Rabaud

Laboratoire Fluides, Automatique et Systèmes Thermiques, Universités Paris-Sud and P. et M. Curie, CNRS (UMR 7608), Bâtiment 502, Campus Universitaire, 91405 Orsay Cedex, France

(Received 30 July 1998)

We report both experimentally and analytically a transition from a convective to an absolute regime for a Kelvin-Helmholtz unstable sheared interface between two fluids in parallel flow in a Hele-Shaw cell. Experimental evidence is obtained by measurements from both sides of this transition, via two independent tests. The results are in good agreement with the nonlinear transition recently described in a theoretical analysis [Couairon and Chomaz, Physica (Amsterdam) **108D**, 236 (1997)]. [S0031-9007(99)08489-6]

PACS numbers: 47.20.Ft, 47.20.Ky, 47.20.Ma, 47.60.+i

The concepts of convective and absolute instabilities have been initially developed in the context of plasma [1], and have been also successfully used in hydrodynamics [2] and optics [3]. These concepts apply as soon as instability waves propagate in the laboratory frame, and open geometry raises the difficult problem of noise or perturbation amplification compared to advection. We study this phenomenon in the case of a hydrodynamic open flow. Open flows, by contrast to closed flows, are characterized by the existence of a mean flow resulting in the advection of all the fluid particles out of the setup. If an instability occurs in such an open flow, it can be either a convective instability (CI) or an absolute instability (AI). A basic property of the CI is that a local flow perturbation in space and time triggers a wave packet that spreads but is advected downstream: after a transient, the perturbation is no more present in a finite setup. In the AI regime, perturbations never leave the system and nonlinear self-sustained structures are observed. The velocity of the rear front of the wave packet in a CI can be deduced from a Ginzburg-Landau (GL) model equation [4,5], but it is only recently that two different scaling laws have been predicted for the growth length of the self-sustained structures existing in an AI [6]. A striking example of flow exhibiting a CI/AI transition is the wake behind an obstacle, where self-sustained structures at a specific intrinsic frequency develop in the so-called Bénard–von Kármán vortex street [7]. In this case, as in most open flow configurations, the flow is nonparallel (the mean-velocity profile is nonuniform in the streamwise direction), and, as the control parameter evolves spatially, local and global descriptions have to be considered [2]. For instance, in classical mixing layer experiments, the shear zone increases downstream by diffusion. However, in heated jets [8] or mixing layer with back flow [9] experiments, the CI/AI transition observed is in good agreement with predictions obtained for parallel velocity profiles [10]. One approach to study the CI/AI transition in an homogeneous basic flow has been to consider a well characterized instability of a closed flow and to superimpose a mean flow, e.g., an open Taylor-Couette or Rayleigh-Bénard setup with through flow [11–13]. In such experiments, the basic instability is governed by a first control parameter, whereas a second parameter (the mean flow) controls the advection of the structures and thus the convective or absolute nature of the instability. In these experiments, permanent structures are observed downstream even in the CI regime. Such structures are called noise-sustained as they result from the spatial amplification of perturbations existing at the inlet. The CI/AI transition was then characterized by the evolution of the temporal spectrum of the structures, from a broad peak corresponding to the behavior of a large band noise amplifier (CI) to a thin peak corresponding to the behavior of an oscillator (AI). Furthermore, the CI/AI transition in these experiments was shown recently to occur linearly [6].

In this Letter, we report the experimental evidence of a nonlinear CI/AI transition in a permanent parallel shear flow when increasing an unique parameter. We choose to realize such a shear between a gas and a liquid in a Hele-Shaw cell (consisting of two plates separated by a small gap) as the geometry inhibits the streamwise evolution of the basic flow. In such cells, much attention has been paid to the normal displacement of one fluid by another: this situation leads to the Saffman-Taylor instability [14] when the displaced fluid is more viscous than the displacing fluid. Less attention has been paid to the dynamics of the interface between two fluids in a parallel flow. Recently, we have shown both experimentally and analytically that the interface becomes Kelvin-Helmholtz unstable when the shear is large enough [15]. We report here measurements of the rear front velocity of an unstable wave packet in the CI regime and of the growth length of the self-sustained structures in the AI regime. These measurements enable us to characterize, both from below and from above, the CI/AI transition.

The Hele-Shaw cell is made of two thick parallel glass plates separated by a thin plastic sheet (thickness $b = 0.35$ mm) delimiting a rectangular cavity (vertical height

 0031-9007/99/82(7)/1442(4)$15.00

$h = 0.1$ m, horizontal length $L = 1.2$ m) where the fluids flow (Fig. 1). Gravity acts in the plane of the cell and is perpendicular to the gas-liquid interface. The gas is nitrogen (viscosity $\mu_{\text{gas}} = 17.5 \times 10^{-6}$ Pa · s and density $\rho_{\text{gas}} = 1.28$ kg · m^{-3}) and the liquid is silicon oil (viscosity $\mu_{\text{liq}} = 0.020$ Pa · s, density $\rho_{\text{liq}} = 952$ kg · m^{-3}, and interfacial tension $\gamma = 0.021$ N · m^{-1}). The two fluids enter the cell, with the gas above the liquid, at a regulated pressure P_{in} and flow out of the cell at a lower pressure P_{out}. The interface position is recorded and analyzed by video means. The pressure difference $\Delta P = P_{\text{in}} - P_{\text{out}}$ can be adjusted in the range 0–10^4 Pa with fluctuations less than 0.2%. At low flow rates, the two fluids flow in parallel with a horizontal interface, and the transverse averaged velocity $\mathbf{u}_i$ of each fluid obeys *below threshold* to Darcy's law: $\mathbf{u}_i = -b^2/(12\ \mu_i)\nabla P$ [14], where i stands for gas or liq. The pressure gradient ∇P being the same for the two fluids everywhere, the velocities U_{gas} and U_{liq} of the basic flow are linked by the relation $\mu_{\text{gas}} U_{\text{gas}} = \mu_{\text{liq}} U_{\text{liq}}$. Because of the strong viscosity contrast, we have $U_{\text{liq}} \ll U_{\text{gas}}$. The typical Reynolds numbers of the flow ($\text{Re}_i = \mu_i U_i b/\rho_i$) are about 10^2 for the gas and 10^{-1} for the liquid and the flow is thus laminar. In such a Hele-Shaw cell, the shear zone does not evolve downstream since the vorticity diffusion is hindered by the small transverse dimension. The width of the shear zone is imposed by the thickness of the cell and is thus constant both in space and time [16]. We look now at the response of the interface to a perturbation for different gas velocities U_{gas}. The interface position can be perturbed locally (at the end of the splitter tongue) by a small variation of the oil injection controlled by an electrovalve.

For a periodic forcing and at low enough U_{gas}, the harmonic perturbation of the interface propagates but is damped [Fig. 2(a)]. At large enough U_{gas}, the linear waves are amplified, become nonlinear in shape [Fig. 2(c)], and saturate further downstream, propagating as periodic localized waves (roughly 3 mm high and 3 mm wide, separated by a distance of a few centimeters). The marginal state is observed [Fig. 2(b)] for the critical velocity $U_{c_{\text{gas}}} = 4.22$ m/s obtained for the most unstable frequency $f = 0.4$ Hz. We will use hereafter the reduced control parameter $\epsilon = (U_{\text{gas}} - U_{c_{\text{gas}}})/U_{c_{\text{gas}}}$.

Let us now present the dynamics of the interface response to a local impulse forcing [17]. This response is sketched in Fig. 3 in a spatiotemporal format where the grey level of one horizontal video line is plotted versus time. This line is taken slightly above (typically 1 mm) the unperturbed interface and recorded any $\Delta t = 1$ s. Hence, in these spatiotemporal images, the waves appear as dark continuous or dashed lines. For $\epsilon < 0$, the initial perturbation is advected but damped [Fig. 3(a)]. For $0 < \epsilon < \epsilon_a$, the perturbation induces a wave packet, whose extension grows in time as several waves appear progressively behind the first one [Fig. 3(b)]. The leading front corresponds to the same leading wave whereas the rear front travels at a much smaller velocity V_r. At larger times, the wave packet is advected by the flow away from the source and out of the cell. This observed unstable state is thus clearly convective. If no other impulse is triggered, the interface remains perfectly flat all along the 1.2 m of the cell. No noise-sustained structures are observed in the setup. When ϵ increases, the velocity V_r decreases: it takes more time for the wave packet to leave the cell and for the interface to return to its unperturbed flat state. Above the value $\epsilon_a = 0.050$, the interface never stays flat, the rear of the packet remaining close to the inlet with a zero mean velocity [Fig. 3(c)]. Note that this is also the case even before the impulse is introduced, as the permanent response to previous perturbations. The distance H from the tip of the splitter tongue over which no sustained waves are observed is defined experimentally as the distance at which the amplitude of the waves reaches one-third of its saturation value [e.g., $H = 8$ cm, in Fig. 3(c)].

In order to characterize the CI/AI transition both from below and above, we have measured V_r in the CI regime (Fig. 4) and H in the other regime (Fig. 5) as a function of ϵ. The rear front velocity V_r decreases when the shear increases (Fig. 4) with the power law predicted by a linearized GL equation [4,5]. However, the rear front velocity is still nonzero when sustained structures appear ($\epsilon = 0.050$) and an extrapolation of the fit gives zero for $\epsilon = 0.142$. For the sustained wave regime, we first have to answer if these waves are noise-sustained or self-sustained. The growth length for noise-sustained structures is known to scale as ϵ^{-1} with a prefactor depending on the noise amplitude [11]. In our case, this scaling does not fit the H variations of Fig. 5. More precisely, we observe that H (sometimes called the healing length [5,11,12]) is small at a large

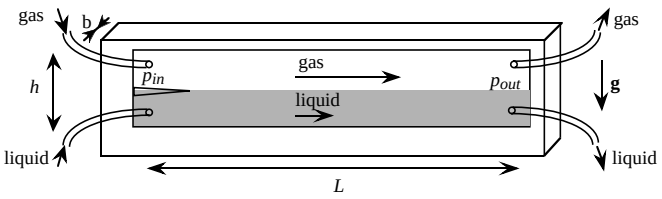

FIG. 1. Experimental Hele-Shaw cell.

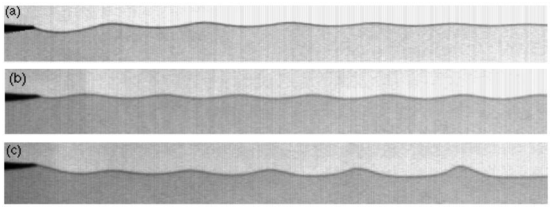

FIG. 2. Snapshots of the interface downstream of the splitter tong (in black): (a) Below threshold for $\epsilon = -0.02$; (b) at threshold ($\epsilon = 0$); and (c) above threshold for $\epsilon = 0.02$. The images are 7 cm long, and the wave velocity is of the order of a few mm/s.

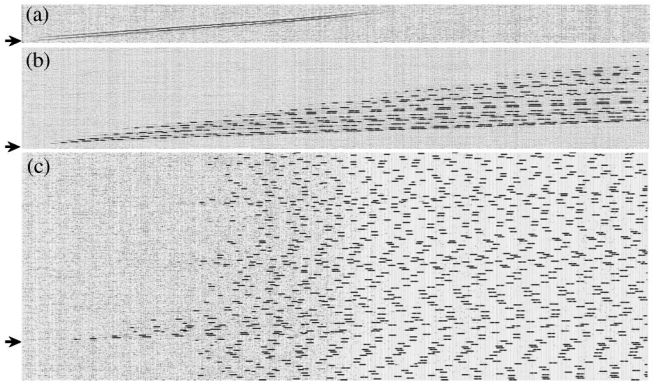

FIG. 3. Spatiotemporal evolution of the interface after a single impulse for (a) $\epsilon = -0.04$, (b) $\epsilon = 0.04$, and (c) $\epsilon = 0.08$. The flow direction is horizontal (only the first 25 cm are displayed) and the time vertical upwards [respectively, (a) 50 s, (b) 130 s, and (c) 270 s]. The dark lines correspond to interfacial waves propagating downstream (from left to right). Each arrow indicates the instant when an impulse has been triggered.

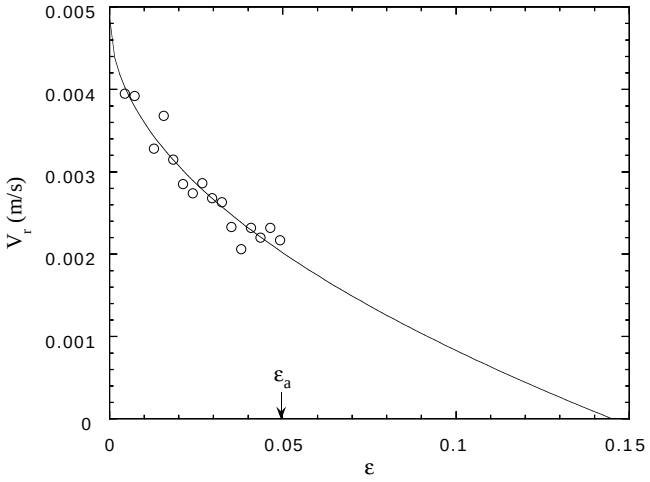

FIG. 4. Rear front velocity V_r as a function of the reduced control parameter ϵ: Experimental measurements (○) and fit (—) derived from a linearized GL equation [4,5], yielding $V_r(\mathrm{m/s}) = 0.0049 - 0.0128\epsilon^{1/2}$.

flow rate, increases when decreasing the shear, and diverges for $\epsilon_a = 0.050$. We can thus conclude that the waves are self-sustained, specific to an AI regime. Furthermore, recent theoretical analysis close above the CI/AI transition [6] predicts that H scales as $(\epsilon - \epsilon_a)^{-1/2}$ when the transition to the AI occurs precisely at the *linearly* predicted CI/AI transition, whereas H scales as $-\ln(\epsilon - \epsilon_a)$ when the *nonlinear* effects cause the transition to the AI to occur before the *linearly* predicted CI/AI transition, thus still in the linear CI regime. The scaling $(\epsilon - \epsilon_a)^{-1/2}$ is found in Ref. [6] to fit well previous data for the healing length obtained in the open Taylor-Couette [5,11] or Rayleigh-Bénard [13] configurations, but no experimental example was known for the scaling $-\ln(\epsilon - \epsilon_a)$. As shown in Fig. 5, we find that our measurements for H are well fitted by the scaling $-\ln(\epsilon - \epsilon_a)$ and not by the scaling $(\epsilon - \epsilon_a)^{-1/2}$. This result demonstrates that the transition to the AI regime is controlled by nonlinearities. Note that we find that the power spectrum of the time signal of our self-sustained structures is not sharp. This is possibly due to the strong nonlinearities that make the wave train unstable because of secondary instabilities.

Let us now present our linear stability analysis of this shear flow. By considering a Haagen-Poiseuille parabolic profile in the gap b of the cell for the velocity $\mathbf{u}$, we have shown [15] that the average of the Navier-Stokes equation through the gap leads to the following two-dimensional equation for the gap-averaged velocity $\overline{\mathbf{u}}$:

$$\frac{\partial \overline{\mathbf{u}}}{\partial t} + \frac{6}{5}(\overline{\mathbf{u}} \cdot \nabla)\overline{\mathbf{u}} = -\frac{1}{\rho}\nabla p - \frac{12\nu}{b^2}\overline{\mathbf{u}}. \qquad (1)$$

Note that for steady parallel flow, the left-hand side of Eq. (1) is zero and the basic flow thus follows Darcy's law.

A Fourier mode analysis assuming small sinewave perturbations $\sim\exp[i(kx - \omega t)]$ superimposed to the basic stationary and unidirectional discontinuous velocity profile leads to the following dispersion relation when taking into account the boundary conditions:

$$\frac{\pi}{4}\gamma k^3 - \frac{6}{5}(\rho_1 U_1^2 + \rho_2 U_2^2)k^2 + \left[\frac{11}{5}(\rho_1 U_1 + \rho_2 U_2)\omega + \Delta\rho g + i\frac{12(\mu_1 U_1 + \mu_2 U_2)}{b^2}\right]k - (\rho_1 + \rho_2)\omega^2 - i\frac{12(\mu_1 + \mu_2)\omega}{b^2} = 0. \qquad (2)$$

The interface between the two fluids (indices 1 and 2) is submitted to the usual continuity of displacement and to a jump in pressure due to surface tension (the $\pi/4$ factor in the surface tension term being due to the permanent transverse curvature of the meniscus [14]). We have already developed the linear stability analysis from a temporal point of view in a recent paper [15]. We give here the spatial approach: the spatial branches $k(\omega)$ are obtained by solving the dispersion relation [Eq. (2)] for complex wave numbers k ($k = k_r + ik_i$), whereas ω is taken real. This choice is suitable when looking for spatial amplification of periodic time disturbances. The real part k_r is the wave number and $-k_i$ is the spatial growth rate. The three spatial branches $-k_i(\omega)$ are plotted in Fig. 6. The direction of propagation of each wave can be determined by studying the sign of k_i for large imaginary part of ω. Two waves propagate downstream and the corresponding branches are called k_1^+ and k_2^+, whereas the third one, k_1^-, propagates upstream. The solution k_2^+ is always stable ($-k_{2i}^+ < 0$) and k_1^+ is stable or unstable

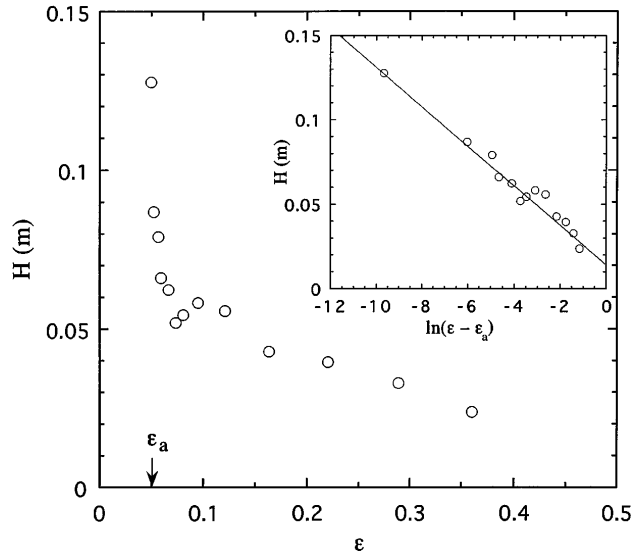

FIG. 5. Healing length H as a function of the reduced control parameter ϵ: Experimental measurements (○) and theoretical fit (—) with the scaling law $-\ln(\epsilon - \epsilon_a)$ in the inset.

depending on the magnitude of the control parameter U_1 and on the frequency range ω. The instability threshold is found to be $U_{1_c} = 4.00\,\mathrm{m/s}$ [Fig. 6(a)] in agreement with our previous temporal linear stability analysis [15]. For higher values of U_1 the two branches k_1^+ and k_1^- deform and pinch off for $\epsilon_a = (U_{1_a} - U_{1_c})/U_{1_c} = 0.069$ [Fig. 6(b)]. This branch pinching at which $\partial\omega/\partial k = 0$ is the signature of the CI/AI transition [2], the nonlinear analysis remaining to be done. These analytical results are thus in good agreement with the experimental part.

In summary, we have studied the experimental impulse response of the interface and found a CI/AI transition when increasing the unique control parameter slightly above the stable/unstable transition. We have characterized well the CI/AI transition both from below and above by measurements of the rear front velocity V_r of the wave packets in the CI regime and of the healing length H of the self-sustained structures in the AI regime. Moreover, the H measurements are well fitted by the scaling $-\ln(\epsilon - \epsilon_a)$, demonstrating that a nonlinear AI regime occurs before the linearly predicted CI/AI transition. This is confirmed by the fact that the value of the control parameter corresponding to the experimental transition ($\epsilon_a = 0.050$) is smaller than the one predicted by the linear stability analysis ($\epsilon_a = 0.069$).

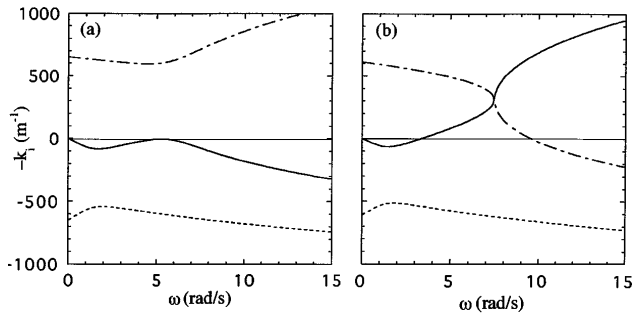

FIG. 6. Theoretical spatial growth rate $-k_i$ for the three branches [$-k_{1i}^+$ (—), $-k_{1i}^-$ (—·—), and $-k_{2i}^+$ (---)] as a function of the wave frequency ω: (a) at the instability threshold for $U_{1_c} = 4.00\,\mathrm{m/s}$ ($\epsilon = 0$) and (b) at the CI/AI transition for $\epsilon_a = 0.069$. The values of ρ_1, ρ_2, μ_1, μ_2, b, g, and γ correspond to the experimental configuration.

We thank F. Charru, J. M. Chomaz, A. Couairon, S. Le Dizès, and P. Huerre for fruitful discussions.

[1] R. J. Briggs *Electron-Stream Interaction with Plasmas* (MIT Press, Cambridge, MA, 1964).
[2] P. Huerre and P. A. Monkewitz, Annu. Rev. Fluid Mech. **22**, 473 (1990).
[3] C. Z. Ning and H. Haken, Phys. Rev. A **41**, 3826 (1990); P. Coullet, L. Gil, and F. Rocca, Opt. Commun. **73**, 403 (1989).
[4] R. J. Deissler, J. Stat. Phys. **40**, 371 (1985); Physica (Amsterdam) **25D**, 233 (1987).
[5] P. Büchel, M. Lücke, D. Roth, and R. Schmitz, Phys. Rev. E **53**, 4764 (1996).
[6] A. Couairon and J. M. Chomaz, Phys. Rev. Lett. **79**, 2666 (1997); Physica (Amsterdam) **108D**, 236 (1997).
[7] G. S. Triantafyllou, K. Kupfer, and A. Bers, Phys. Rev. Lett. **59**, 1914 (1987); G. S. Triantafyllou, M. S. Triantafyllou, and C. Chryssostomidis, J. Fluid Mech. **170**, 461 (1986).
[8] K. R. Sreenivasan, S. Raghu, and D. Kyle, Exp. Fluids **7**, 309 (1987).
[9] P. J. Strykowsky and D. L. Niccum, Phys. Fluids A **4**, 770 (1992).
[10] P. Huerre and P. A. Monkewitz, J. Fluid Mech. **159**, 151 (1985); G. S. Triantafyllou, Phys. Fluids **6**, 164 (1994).
[11] A. Tsameret and V. Steinberg, Europhys. Lett. **14**, 331 (1991); Phys. Rev. Lett. **67**, 3392 (1991); Phys. Rev. E **49**, 1291 (1994).
[12] K. L. Babcock, G. Ahlers, and D. S. Cannell, Phys. Rev. Lett. **67**, 3388 (1991); Phys. Rev. E **50**, 3670 (1994).
[13] H. W. Müller, M. Lücke, and M. Kamps, Europhys. Lett. **10**, 451 (1989); Phys. Rev. A **45**, 3714 (1992).
[14] G. M. Homsy, Annu. Rev. Fluid Mech. **19**, 271 (1987).
[15] P. Gondret and M. Rabaud, Phys. Fluids **9**, 3267 (1997).
[16] P. Gondret, N. Rakotomalala, M. Rabaud, D. Salin, and P. Watzky, Phys. Fluids **9**, 1841 (1997).
[17] Experimentally, a slight liquid injection overpressure ($\delta P = 5$ Pa) during one second results in an initial deformation of the interface with a typical width 5 mm and amplitude 0.5 mm at the end of the splitter tongue. This amplitude has been chosen for a visualization purpose, but similar results are obtained for much smaller amplitudes.